# Topological phase for spin-orbit transformations on a laser beam

C. E. R. Souza[†], J. A. O. Huguenin[†], P. Milman[††], and A.Z. Khoury[†]
[†] *Instituto de Física, Universidade Federal Fluminense, 24210-340 Niterói - RJ, Brasil. and*
[††] *Laboratoire Matériaux et Phenomènes quantiques CNRS UMR 7162, Université Denis Diderot, 2 Place Jussieu 75005 Paris cedex.*

We investigate the topological phase associated with the double connectedness of the $SO(3)$ representation in terms of maximally entangled states. An experimental demonstration is provided in the context of polarization and spatial mode transformations of a laser beam carrying orbital angular momentum. The topological phase is evidenced through interferometric measurements and a quantitative relationship between the concurrence and the fringes visibility is derived. Both the quantum and the classical regimes were investigated.

PACS numbers: PACS: 03.65.Vf, 03.67.Mn, 07.60.Ly, 42.50.Dv



The seminal work by S. Pancharatnam [1] introduced for the first time the notion of a geometric phase acquired by an optical beam passing through a cyclic sequence of polarization transformations. A quantum mechanical parallel for this phase was later provided by M. Berry [2]. Recently, the interest for geometric phases was renewed by their potential applications to quantum computation. The experimental demonstration of a conditional phase gate was recently provided both in nuclear magnetic ressonance [3] and trapped ions [4]. Another optical manifestation of geometric phase is the one acquired by cyclic spatial mode conversions of optical vortices. This kind of geometric phase was first proposed by van Enk [5] and recently found a beautiful demonstration by E. J. Galvez *et al* [6].

The Hilbert space of a single qubit admits an useful geometric representation of pure states on the surface of a sphere. This is the Bloch sphere for spin 1/2 particles or the Poincaré sphere for polarization states of an optical beam. A Poincaré sphere representation can also be constructed for the first order subspace of the spatial mode structure of an optical beam [7]. Therefore, in the quantum domain, we can attribute two qubits to a single photon, one related to its polarization state and another one to its spatial structure. Geometrical phases of a cyclic evolution of the mentioned states can be beautifully interpreted in such representations as being related to the solid angle of a closed trajectory. However, in order to compute the total phase gained in a cyclic evolution, one should also consider the dynamical phase. When added to the geometrical phase, it leads to a total phase gain of $\pi$ after a cyclic trajectory. This phase has been put into evidence for the first time using neutron interference [8]. The appearence of this $\pi$ phase is due to the double connectedness of the three dimensional rotation group $SO(3)$. However, in the neutron experience, only two dimensional rotations were used, and this topological property of $SO(3)$ was not unambiguously put into evidence, as explained in details in [9, 10].

As discussed by P. Milman and R. Mosseri [9, 11], when the quantum state of two qubits is considered, the mathematical structure of the Hilbert space becomes richer and the phase acquired through cyclic evolutions demands a more careful inspection. The naive sum of independent phases, one for each qubit, is applicable only for product states. In this case, the two qubits are geometrically represented by two independent Bloch spheres. When a more general partially entangled *pure* state is considered, the phase acquired through a cyclic evolution has a more complex structure and can be separated in three contributions: dynamical, geometrical and topological. Maximally entangled states are solely represented on the volume of the $SO(3)$ sphere which has radius $\pi$ and its diametrically opposite points identified. This construction reveals two kinds of cyclic evolutions, each one mapped to a different homotopy class of closed trajectories in the $SO(3)$ sphere. One kind is mapped to closed trajectories that do not cross the surface of the sphere ($0-$type) and the other one is mapped to trajectories that cross the surface ($\pi-$type). The phase acquired by a maximally entangled state is 0 for the first kind and $\pi$ for the second one.

In the present work we demonstrate the topological phase associated to polarization and spatial mode transformations of an optical vortice. This phase appears first in the classical description of a paraxial beam with arbitrary polarization state and has its quantum mechanical counterpart in the spin-orbit entanglement of a single photon, which constitutes one possible realization of a two-qubit system and the topological phase discussed in Ref.[9]. However, it is interesting to observe that, like the Pancharatnam phase, the two-qubit topological phase also admits a classical manifestation, since it can be implemented on the classical amplitude of the optical field. This is also the first experiment unambiguously showing the double connectedness of the rotation group $SO(3)$. The optical modes used in our experiment have a mathematical structure analog to the one of entangled states, so that the geometrical representation developped in [10] also applies and the results of Ref.[9, 11] can be experimentally demonstrated. When excited with single photons, these modes give rise to single particle entangled

states and provide a more direct relationship with the ideas put forward in Refs.[9, 10, 11]. This regime is also investigated in the present work. There are a number of quantum computing protocols that can be implemented with single particle entanglement and will certainly benefit from our results.

Let us now combine the spin and orbital degrees of freedom in the framework of the classical theory in order to build the same geometric representation applicable to a two-qubit quantum state. Consider a general first order spatial mode with arbitrary polarization state:

$$\begin{aligned}\mathbf{E}(\mathbf{r}) &= \alpha\psi_+(\mathbf{r})\hat{e}_H + \beta\psi_+(\mathbf{r})\hat{e}_V + \gamma\psi_-(\mathbf{r})\hat{e}_H \\ &+ \delta\psi_-(\mathbf{r})\hat{e}_V \ , \end{aligned} \tag{1}$$

where $\hat{e}_{H(V)}$ are two linear polarization unit vectors along two orthogonal directions $H$ and $V$, and $\psi_\pm(\mathbf{r})$ are the normalized first order Laguerre-Gaussian profiles which are orthogonal solutions of the paraxial wave equation [12]. We may now define two classes of spatial-polarization modes: the separable (S) and the nonseparable (NS) ones. The S modes are of the form

$$\mathbf{E}(\mathbf{r}) = \left(\alpha_+\psi_+(\mathbf{r}) + \alpha_-\psi_+(\mathbf{r})\right)\left(\beta_H\hat{e}_H + \beta_V\hat{e}_V\right) \ . \tag{2}$$

For these modes, a single polarization state can be atributted to the whole wavefront of the paraxial beam. They play the role of separable two-qubit quantum states.

For nonseparable (NS) paraxial modes, the polarization state varies across the wavefront. As for entanglement in two-qubit quantum states, the separability of a paraxial mode can be quantified by the analogous definition of concurrence. For the spin-orbit mode described by Eq.(1), it is given by:

$$C = 2 \mid \alpha\delta - \beta\gamma \mid \ . \tag{3}$$

Let us first consider the maximally nonseparable modes (MNS) of the form

$$\begin{aligned}\mathbf{E}(\mathbf{r}) &= \alpha\psi_+(\mathbf{r})\hat{e}_H + \beta\psi_+(\mathbf{r})\hat{e}_V - \beta^*\psi_-(\mathbf{r})\hat{e}_H \\ &+ \alpha^*\psi_-(\mathbf{r})\hat{e}_V \ . \end{aligned} \tag{4}$$

For these modes $C = 1$. It is important to mention that the concept of entanglement does not applies to the MNS mode, since the object described by Eq.(4) is not a quantum state, but a classical amplitude. However, we can build an $SO(3)$ representation of the MNS modes as it was done in Refs.[11, 13]. Let us define the following normalized MNS modes:

$$\begin{aligned}\mathbf{E_1}(\mathbf{r}) &= \frac{1}{\sqrt{2}}\left[\psi_+(\mathbf{r})\hat{e}_H + \psi_-(\mathbf{r})\hat{e}_V\right] \ , \\ \mathbf{E_2}(\mathbf{r}) &= \frac{-i}{\sqrt{2}}\left[\psi_+(\mathbf{r})\hat{e}_H - \psi_-(\mathbf{r})\hat{e}_V\right] \ , \\ \mathbf{E_3}(\mathbf{r}) &= \frac{-i}{\sqrt{2}}\left[\psi_+(\mathbf{r})\hat{e}_V + \psi_-(\mathbf{r})\hat{e}_H\right] \ , \\ \mathbf{E_4}(\mathbf{r}) &= \frac{1}{\sqrt{2}}\left[\psi_+(\mathbf{r})\hat{e}_V - \psi_-(\mathbf{r})\hat{e}_H\right] \ . \end{aligned} \tag{5}$$

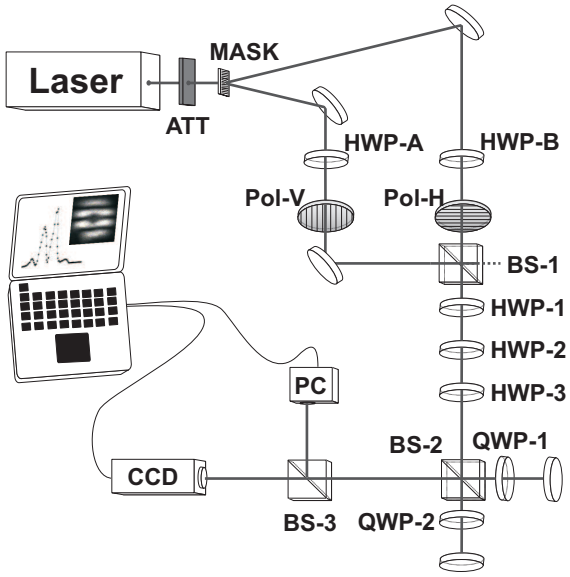


FIG. 1: Experimental setup.

The $SO(3)$ sphere is then constructed in the following way: mode $\mathbf{E_1}$ is represented by the center of the sphere, while modes $\mathbf{E_2}$, $\mathbf{E_3}$, and $\mathbf{E_4}$ are represented by three points on the surface, connected to the center by three mutually orthogonal segments. Each point of the $SO(3)$ sphere corresponds to a MNS mode. Following the recipe given in Ref.[13], the coefficients $\alpha$ and $\beta$ of Eq.(4) are parametrized to:

$$\begin{aligned}\alpha &= \cos\frac{a}{2} - i\,k_z\,\sin\frac{a}{2} \ , \\ \beta &= -(k_y + i\,k_x)\,\sin\frac{a}{2} \ , \end{aligned} \tag{6}$$

where $(k_x, k_y, k_z) = \mathbf{k}$ is a unit vector, and $a$ is an angle between 0 and $\pi$. With this parametrization, each MNS mode is represented by the vector $a\,\mathbf{k}$ in the sphere.

In order to evidence the topological phase for cyclic transformations, we must follow two different closed paths, each one belonging to a different homotopy class, and compare their phases. The experimental setup is sketched in Fig.(1). First, a linearly polarized $\mathrm{TEM}_{00}$ laser mode is diffracted on a forked grating used to generate Laguerre-Gaussian beams [14]. The two side orders carrying the $\psi_+(\mathbf{r})$ and $\psi_-(\mathbf{r})$ spatial modes are transmitted through half waveplates HWP-A and HWP-B, followed by two orthogonal polarizers Pol-V and Pol-H, and finally recombined at a beam splitter (BS-1). Half waveplates HWP-A and HWP-B are oriented so that their fast axis are paralell. This allows us to adjust the mode separability at the output of BS-1 without changing the corresponding output power, what prevents normalization issues.

Experimentally, an MNS mode is produced when both HWP-A and HWP-B are oriented at $22.5^o$, so that the

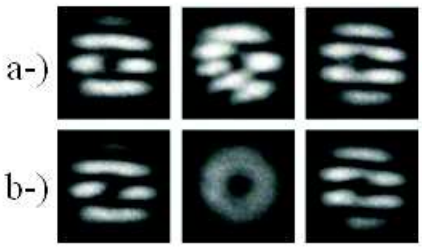


FIG. 2: Interference patterns for a-) a maximally nonseparable, and b-) a separable mode. From left to right the images were obtained with QWP-2 oriented at $-45^o$, $0^o$, and $45^o$, respectively.

setup prepares mode $\mathbf{E_1}$ located at the centre of the sphere. Other MNS modes can then be obtained by unitary transformations in only one degree of freedom. Since polarization is far easier to operate than spatial modes we choose to implement the cyclic transformations in the $SO(3)$ sphere using waveplates. The MNS mode $\mathbf{E_1}$ is first transmitted through three waveplates. The first one (HWP-1) is oriented at $0^o$ and makes the transformation $\mathbf{E_1} \rightarrow \mathbf{E_2}$, the second one (HWP-2) is oriented at $-45^o$ and makes the transformation $\mathbf{E_2} \rightarrow \mathbf{E_3}$, and the third one (HWP-3) is oriented at $90^o$ and makes the transformation $\mathbf{E_3} \rightarrow \mathbf{E_4}$. Finally, two alternative closures of the path are performed in a Michelson interferometer. In one arm a $\pi-$type closure is implemented by double pass through a quarter-waveplate (QWP-1) fixed at $-45^o$. In the other arm, either a $0-$type or a $\pi-$type closure is performed by a double pass through another quarter-waveplate (QWP-2) oriented at a variable angle between $-45^o$ ($\pi-$type) and $45^o$ ($0-$type). These trajectories are analogous to spin rotations around different directions of space [13]. They evidence the topological properties of the three dimensional rotation group.

In order to provide spatial interference fringes, the interferometer was slightly misaligned. The interference patterns were registered with either a charge coupled device (CCD) camera or a photocounter (PC), depending on the working power. First, we registered the interference patterns obtained when an intense beam is sent through the apparatus. The images shown in Fig.(2a) demonstrate clearly the $\pi$ topological phase shift. The phase singularity characteristic of Laguerre-Gaussian beams can be easily identified in the images and is very useful to evidence the phase shift. When both arms perform the same kind of trajectory in the $SO(3)$ sphere (QWP-1 and QWP-2 oriented at $-45^o$), a bright fringe falls on the phase singularity. When QWP-2 is oriented at $45^o$, the trajectory performed in each arm belongs to a different homotopy class and a dark fringe falls on the singularity, what clearly demonstrates the $\pi$ topological phase shift.

In order to discuss the role played by mode separability, it is interesting to observe the pattern obtained when QWP-2 is oriented at intermediate angles, which correpond to open trajectories in the $SO(3)$ sphere. We observed that during the phase shift transition, the interference fringes are deformed and finally return to its initial topology with the $\pi$ phase shift. This is clearly illustrated by the intermediate image displayed in Fig.(2a), which corresponds to QWP-2 oriented at $0^o$ . Notice that, despite the deformation, the interference fringes display high visibility.

As we mentioned above, the mode preparation settings can be adjusted in order to provide a separable mode. For example, when we set HWP-A and B both at $45^o$ , the output of BS-1 is the separable mode $\psi_+(\mathbf{r})\hat{e}_H$ , which can be represented in the Poincaré spheres for spatial and polarization modes. The same $\pi$ phase shift can be observed when QWP-2 is rotated, but the transition is essentially different. The intereference pattern is not topologically deformed, but its visibility decreases until it completelly vanishes at $0^o$ , and then reappears with the $\pi$ phase shift. This transition is clearly illustrated by the three patterns displayed in Fig.(2b). In this case, the $\pi$ phase shift is of purely geometric nature, since the spatial mode is kept fixed while the polarization mode is turned around the equator of the corresponding Poincaré sphere.

The relationship between mode separability and fringes visibility can be clarified by a straightforward calculation of the interference pattern. Therefore, let us consider that HWP-A and B are oriented so that the output of BS-1 is described by

$$\mathbf{E}_\epsilon(\mathbf{r}) = \sqrt{\epsilon}\,\psi_+(\mathbf{r})\hat{e}_H + \sqrt{1-\epsilon}\,\psi_-(\mathbf{r})\hat{e}_V \ , \qquad (7)$$

where $\epsilon$ is the fraction of the $\psi_+(\mathbf{r})\hat{e}_H$ mode in the output power. Now, let us consider that QWP-2 is oriented at $0^o$ and suppose that the two arms of the Michelson interferometer are slightly misaligned so that the wave vectors difference between the two outputs is $\delta\mathbf{k} = \delta k\,\hat{x}$ , orthogonal to the propagation axis. Taking into account the passage through the three half waveplates, and the transformation performed in each arm of the Michelson interferometer, we arrive at the following expression for the interference pattern:

$$I(\mathbf{r}) = 2\,|\psi(\mathbf{r})|^2\left[1 + 2\sqrt{\epsilon(1-\epsilon)}\sin 2\phi \sin\left(\delta k\, x\right)\right] \ , \quad (8)$$

where $\phi = \arg(x+iy)$ is the angular coordinate in the transverse plane of the laser beam, and $|\psi(\mathbf{r})|^2$ is the doughnut profile of the intensity distribution of a Laguerre-Gaussian beam. It is clear from Eq.(8) that the visibility of the interference pattern is $2\sqrt{\epsilon(1-\epsilon)}$, which is precisely the concurrence of $\mathbf{E}_\epsilon(\mathbf{r})$ as given by Eq.(3). Therefore, the fringes visibility is quantitatively related to the separability of the mode sent through the setup. However, the numerical coincidence with the concurrence

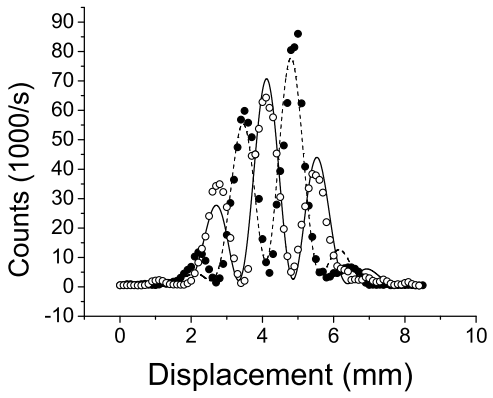


FIG. 3: Interference patterns measured in the photocounting regime for $\epsilon = 1/2$. Empty and full circles correspond to QWP-2 oriented at $-45^o$ and $45^o$, respectively. Solid and dashed lines are theoretical fits with sinusoidal functions modulated by a Laguerre-Gaussian envelope. The phase shift given by the fits is $3.14\,rad$.

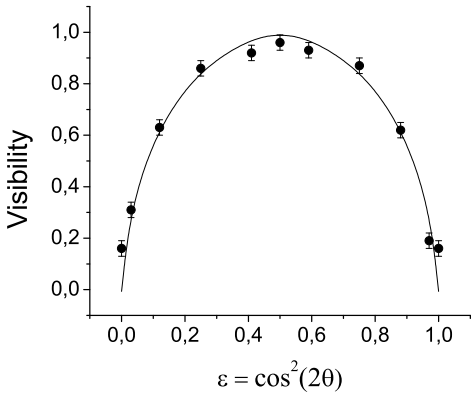


FIG. 4: Fringes visibility as a function of $\epsilon$. The solid line is a theoretical fit with $C = 2\sqrt{\epsilon(1-\epsilon)}$.

is restricted to modes of the form given by Eq.(7). In fact, it is important to stress that the fringes visibility cannot be regarded as a measure of the concurrence for *any* nonseparable mode, but for our purposes it evidences the topological nature of the phase shift implemented by the experimental setup. A detailed discussion on the measurement of the concurrence is available in Ref.[15].

Next, we briefly discuss the quantum domain. When a partially nonseparable mode like $\mathbf{E}_\epsilon(\mathbf{r})$ is occupied by a single photon, this leads to partially entangled single particle quantum states of the kind

$$|\varphi_\epsilon\rangle = \sqrt{\epsilon}\,|+H\rangle + \sqrt{1-\epsilon}\,|-V\rangle\ . \qquad (9)$$

Experimentally, we attenuated the laser beam down to the single photon regime, and scanned a photocounting module across the interference pattern. First, HWP-A and B were set at $22.5^o$ ($\epsilon = 1/2$) in order to evidence the topological phase in this regime. Fig.(3) displays the interference patterns obtained with QWP-2 oriented at $-45^o$ and $45^o$. The $\pi$ phase shift is again clear.

The relationship between the fringes visibility and the state separability was evidenced by fixing QWP-2 at $0^o$ and rotating HWP-A and B by an angle $\theta$ so that $\epsilon = \cos^2 2\theta$. Fig.(4) shows the experimental results for the fringes visibility for several values of $\epsilon$. The solid line corresponds to the analytical expression of the concurrence, showing a very good agreement with the experimental values.

As a conclusion, we demonstrated the double connected nature of the $SO(3)$ rotation group and the topological phase acquired by a laser beam passing through a cycle of spin-orbit transformations. We investigated both the classical and the quantum regimes and compared the separability of the mode travelling through the apparatus with the visibility of the interference fringes. Our results may constitute an useful tool for quantum computing and quantum information protocols.

The authors are deeply grateful to S.P. Walborn and P.H. Souto Ribeiro for their precious help with the photocounting system and for fruitful discussions. Funding was provided by Coordenação de Aperfeiçoamento de Pessoal de Nível Superior (CAPES), Fundação de Amparo à Pesquisa do Estado do Rio de Janeiro (FAPERJ-BR), and Conselho Nacional de Desenvolvimento Científico e Tecnológico (CNPq).

[1] S. Pancharatnam, Proc. Ind. Acad. Sci. **44**, 247 (1956).
[2] M. V. Berry, Proc. R. Soc. London A **392**, 45 (1984).
[3] J. A. Jones, V. Vedral, A. Ekert, and G. Castagnoli, Nature (London) **4**03, 869 (2000).
[4] L.-M. Duan, J. I. Cirac, and P. Zoller, Science **2**92, 1695 (2001).
[5] S.J. van Enk, Opt. Comm. **102**, 59 (1993).
[6] E. J. Galvez *et al*, Phys. Rev. Lett. **90**, 203901 (2003).
[7] M. J. Padgett and J. Courtial, Opt. Lett. **24**, 430 (1999).
[8] S. A. Werner *et al*, Phys. Rev. Lett. **35**, 1053 (1975).
[9] P. Milman, and R. Mosseri, Phys. Rev. Lett. **90**, 230403 (2003).
[10] R. Mosseri, and R. Dandoloff, J. Phys. A **34**, 10243 (2003).
[11] P. Milman, Phys. Rev. A **73**, 062118 (2006).
[12] A. Yariv, "Quantum Electronics", John Wiley & Sons, third ed. (1988).
[13] W. LiMing, Z. L. Tang, and C. J. Liao, Phys. Rev. A **69**, 064301 (2004).
[14] N. R. Heckenberg, R. McDuff, C. P. Smith, and A. G. White, Opt. Lett. **17**, 221 (1992); G.F. Brand, Am. J. of Phys. **67**, 55 (1999).
[15] S. Walborn, P. H. Souto Ribeiro, L. Davidovich, F. Mintert, and A. Buchleitner, Nature **440**, 1022 (2006).